Observation of Helium in Mercury's Exosphere by PHEBUS on Bepi-Colombo

Eric Quémerais, Dimitra Koutroumpa, Rosine Lallement, Bill R Sandel, Rozenn Robidel, Jean-Yves Chaufray, Aurélie Reberac, François Leblanc, Ichiro Yoshikawa, Kazuo Yoshioka, et al.

JGR Planets

RESEARCH ARTICLE
10.1029/2023JE007743

Observation of Helium in Mercury's Exosphere by PHEBUS on Bepi-Colombo

Eric Quémerais[1], Dimitra Koutroumpa[1], Rosine Lallement[2], Bill R. Sandel[3], Rozenn Robidel[1], Jean-Yves Chaufray[1], Aurélie Reberac[1], Francois Leblanc[1], Ichiro Yoshikawa[4], Kazuo Yoshioka[4], Go Murakami[5], Oleg Korablev[6], Denis Belyaev[6], Maria G. Pelizzo[7], and Alain J. Corso[8]

[1]LATMOS-OVSQ, Université Versailles Saint-Quentin, Guyancourt, France, [2]GEPI, Observatoire de Paris, Université Paris Sciences et Lettres (PSL), Paris, France, [3]Lunar and Planetary Laboratory, University of Arizona, Tucson, AZ, USA, [4]Tokyo University, Tokyo, Japan, [5]Institute of Space and Astronautical Science, Japan Aerospace Exploration Agency, Sagamihara, Japan, [6]IKI, Moscow, Russia, [7]Department of Information Engineering, University of Padova, Padova, Italy, [8]National Research Council of Italy, Institute for Photonics and Nanotechnologies, Padova, Italy

Key Points:

- This paper presents helium measurements obtained during the first flyby of Mercury by the Bepi-Colombo mission
- Calibrations of UVS/Mariner 10 and of PHEBUS are cross-checked with observations of the interplanetary glow at 58.4 nm
- The helium content in the exosphere of Mercury derived by PHEBUS is 4.5–7.5 times lower than the previous estimate from the Mariner 10 mission

Correspondence to:
E. Quémerais,
Eric.quemerais@latmos.ipsl.fr

Citation:
Quémerais, E., Koutroumpa, D., Lallement, R., Sandel, B. R., Robidel, R., Chaufray, J.-Y., et al. (2023). Observation of helium in Mercury's exosphere by PHEBUS on Bepi-Colombo. *Journal of Geophysical Research: Planets*, *128*, e2023JE007743. https://doi.org/10.1029/2023JE007743

Received 16 JAN 2023
Accepted 18 MAY 2023

Abstract On 1 October 2021, Bepi-Colombo performed its first flyby of Mercury. During the maneuver, the short wavelength channel (55–155 nm) of "Probing the Hermean Exosphere by UV Spectroscopy" (PHEBUS) was activated for a total duration of 1 hr. The helium resonance line at 58.4 nm was clearly observed during the whole sequence. At large distance from the planet, the emission was due to helium atoms in the interplanetary medium (interplanetary UV glow). Just after crossing the terminator of the planet and entering the dawn side of the exosphere, PHEBUS observed a clear additional emission due to scattering of solar photons by helium atoms in the exosphere of Mercury. The first detection of the 58.4 nm line in the exosphere of Mercury was reported by Broadfoot et al. (1976, https://doi.org/10.1029/gl003i010p00577) following the Mariner 10 flybys in 1974. The PHEBUS observation of exospheric helium emissions is the first for this element since the UVS measurements. In this paper, we present the results of our analysis of the PHEBUS data at 58.4 nm. Calibration of both instruments are compared with observations of the interplanetary glow, showing that the measurements of both instruments are accurate. However, we find that the exospheric density of helium atoms deduced from the PHEBUS data is 4.5–7.5 times lower than the previous estimate from UVS on Mariner 10. Possible explanations are considered. We show that some of the helium atoms present in the exosphere of Mercury could originate from the local interstellar cloud.

Plain Language Summary On 1 October 2021, The Bepi-Colombo mission performed its first flyby of Mercury. During this maneuver, the "Probing the Hermean Exosphere by UV Spectroscopy" (PHEBUS) ultraviolet spectrometer was activated for 1 hour, starting 30 min before the time of the closest approach to the surface of Mercury. This instrument is able to measure the emission of helium atoms either in the interplanetary medium or in the tenuous atmosphere of Mercury. The presence of helium atoms around Mercury was first discovered by the ultraviolet spectrograph (UVS) of the Mariner 10 mission in 1974. The observations of PHEBUS confirm the detection of helium atoms in the atmosphere of Mercury. However, the amount of helium atoms detected by PHEBUS is 4.5–7.5 times lower than the value reported by UVS after the Mariner 10 flybys. We discuss possible explanations for this difference.

1. Introduction

The Bepi-Colombo mission is an international cooperation between the European Space Agency, ESA, and the Japan Aerospace Exploration Agency, JAXA. Its aim is to study Mercury and its environment. It has been launched in October 2018 and is composed of two satellites that will be put in orbit at the end of 2025. PHEBUS, an acronym for Probing the Hermean Exosphere By Ultraviolet Spectroscopy, is an ultraviolet spectrograph on board ESA's Mercury Planetary Orbiter (MPO). The main objective of this instrument is to study the Hermean exosphere and its interactions with the surface and the solar wind.

The primary objectives and design of PHEBUS are described by Chassefière et al. (2010). Quémerais et al. (2020) gave an early report on the status of PHEBUS based on ground calibration activities. Since the post-launch commissioning activities of 2019, PHEBUS has performed observations of stars, planetary objects (Moon and Venus) and the interplanetary background. On 1 October 2021, Bepi-Colombo performed its first flyby of

Mercury. During this maneuver, the short wavelength UV channel of PHEBUS was activated covering the closest part of the approach to the planet.

Here we report the results obtained for the 58.4 nm spectral line which corresponds to the emission of helium atoms present in the exosphere of Mercury. This is the first measurement of this emission since the flybys of Mercury by Mariner 10 in 1974.

Our aim is to compare the measurements of PHEBUS at 58.4 nm with the results of UVS/Mariner 10 reported by Broadfoot et al. (1976). First, we show how we have reconstructed the value of the excitation rate at 58.4 nm over the whole period from 1974 to 2021. Then we use observations of the interplanetary UV background at 58.4 nm to calibrate both instruments. Finally we compare the results obtained at 58.4 nm by both instruments in the exosphere of Mercury.

2. Excitation Rate at 58.4 nm

Helium atoms in the interplanetary medium and in the exospheres of planets are illuminated by the solar line at 58.4 nm. This line, like many other ultraviolet solar lines, varies strongly with solar rotation and during the 11-year solar activity cycle (Woods et al., 2012). To derive the column density of helium atoms present in the exosphere of Mercury, it is therefore necessary to know the excitation rate of the 58.4 nm line at the time of observation.

The line width of the solar line at 58.4 nm has been estimated by different authors with values ranging from 0.0016 to 0.015 nm, for example, Yoneda et al. (2021). In the discussion section, we will come back to this topic and show why the lower values are not in agreement with observations of the interplanetary helium background. Here, we will follow McMullin et al. (2004) and Lallement et al. (2004) and assume a value of 0.0136 nm, which is the average of the SUMER/SOHO measurements (Wilhelm et al., 1997). Note that the SUMER measurements did not show a consistent variation with the solar activity cycle. The total flux of the 58.4 nm line flux has been measured by CDS (Coronal Diagnostics Spectrometer) on SOHO from 1997 to 2001 (McMullin et al., 2004) and by EVE (EUV Variability Experiment) on SDO since 2010 (Woods et al., 2012). Both flux measurements are in good agreement for solar minimum conditions, although, it seems there is a difference for peak values at solar activity maximum. This is not an issue in this work, however. Both Mariner 10 and Bepi-Colombo measurements discussed here took place within a few months of solar activity minimum. The CDS values are given in McMullin et al. (2004) and have been used to create a proxy based on the solar MgII activity index. Using the expressions given in the Appendix A for the line center flux and for the excitation rate, we have been able to reconstruct the excitation rate at 1 AU for 58.4 nm from 1973 to 2022, shown in Figure 1. Following the Messenger flybys, Killen et al. (2009) have estimated excitations rates for some known or expected exospheric lines. The authors computed the values for the first two Messenger flybys (Table 1 of that paper). When corrected for distance, we see that our results for the 58.4 nm excitation rate at 1 AU are slightly higher than the values given in that paper. Similarly, the estimates of the excitation rate for the Mariner 10 flybys given in Broadfoot et al. (1976) or Yoneda et al. (2021) are in general agreement with the values shown in Figure 1.

From this reconstruction, we see that the excitation rate at 1 AU can vary by more than a factor of 2 during the 11-year solar activity cycle. The Mariner 10 flybys happened just before a solar activity minimum and the Bepi-Colombo first flyby of Mercury in October 2021 was performed after the most recent minimum in 2019. We find that the excitation rate at the time of the Bepi-Colombo flyby is 30% higher than at the time of the Mariner 10 flybys.

3. Helium in the Interplanetary Medium

The interplanetary helium (IPHe) resonance glow at 58.4 nm has been observed by various space experiments since the 1970s. The first observations were made with the STP-72 rocket experiment (Weller & Meier, 1974). Like hydrogen atoms in the interplanetary medium, helium atoms originate from the local cloud and can reach the inner heliosphere because of the relative motion between the Sun and the Local Cloud. In the inner heliosphere, these helium atoms can resonantly backscatter the solar photons at 58.4 nm which create a glow that is observed in all directions in the sky.

In 1973 and 1974, the Ultraviolet Spectrograph (UVS) observed the interplanetary helium glow while Mariner 10 was performing a series of Roll Calibration Maneuvers (RCM). These data were described and analyzed by Kumar and Broadfoot (1979).

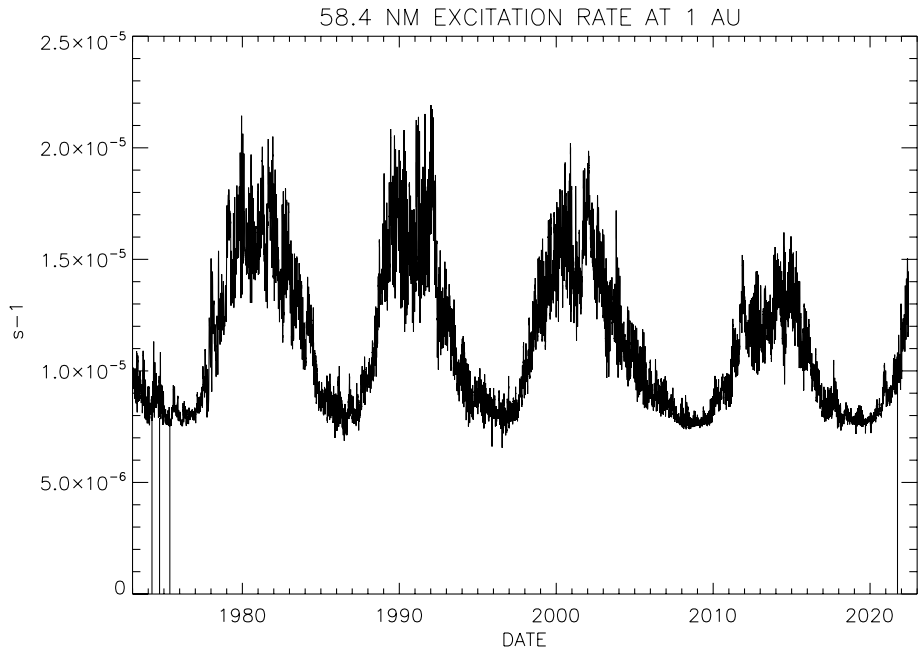

Figure 1. Values of the excitation rate at 1 AU for the helium 58.4 nm line from 1973 to 2022. The dates for the 3 Mariner 10 (29 March 1974, 21 September 1974 and 16 May 1975) and the Bepi-Colombo (1 October 2021) flybys are shown. All of these flybys were performed close to a minimum of solar activity. These values are based on the correlation between the solar MgII index and the solar flux at 58.4 nm as given by McMullin et al. (2004).

Similarly, in 2021, PHEBUS on Bepi-Colombo performed 13 observations of the interplanetary background at 58.4 nm. Figure 2 presents a typical spectrum recorded by the EUV channel when observing the interplanetary ultraviolet background. The spectrum shows the three main lines that can be observed, the H Lyman α and H Lyman β lines and the He 58.4 nm line. This spectrum was obtained with the large aperture of PHEBUS which has dimensions of $1.4° \times 3.1°$ while the slit has dimensions of $0.1° \times 2°$. Using the large aperture increases the count rate by a factor 20 but degrades the spectral resolution from 1 to 14 nm, which is not an issue here.

In the following sections, we will use the model presented by Lallement et al. (2004) to analyze the observations of both UV instruments. This model was developed to fit the data of Prognoz 5/6 (Dalaudier et al., 1984) and EUVE (Vallerga et al., 2004). It is consistent with our current knowledge of the helium parameters in the local cloud (Möbius et al., 2004).

This analysis will allow us to derive the theoretical calibration factor of both instruments. These theoretical values will be compared to measured values to check whether the two data sets give a consistent view of the interplanetary helium glow.

Table 1
Parameters of the Mariner 10 Roll Calibration Maneuvers

RCM #	Date	Distance (AU)	Ecliptic lon (°)	Excitation rate (s^{-1})	Derived ratio (counts per Rayleigh)
1	1973-11-06	0.981	43.8	0.80×10^{-5}	0.41 ± 0.08
2	1973-12-07	0.906	71.7	0.77×10^{-5}	0.41 ± 0.08
3	1973-12-19	0.882	82.3	0.87×10^{-5}	0.41 ± 0.07
4	1974-01-28	0.769	130.7	0.76×10^{-5}	0.45 ± 0.08

3.1. Calibration of UVS Helium Channel

The Mariner 10 UVS Interplanetary helium (IP He) glow data are presented in Kumar and Broadfoot (1979). Our aim is to re-analyze these data to check the UVS calibration factor for the helium Channel. The same analysis will be performed with the PHEBUS IP He observations.

The Mariner 10 Roll Calibration Maneuver (RCM) data analyzed by Kumar and Broadfoot (1979) are available from the NSSDC Archive (id PSPA-00315), see acknowledgments for details. The data set consists of 4 files for 6 November, 7 December, 19 December 1973, and 28 January 1974. Each file contains between 978 and 1050 lines corresponding to each individual measurement. The records give the boresight in equatorial coordinates and the count rate for channels 2, 5, and 9 which correspond to dark counts,

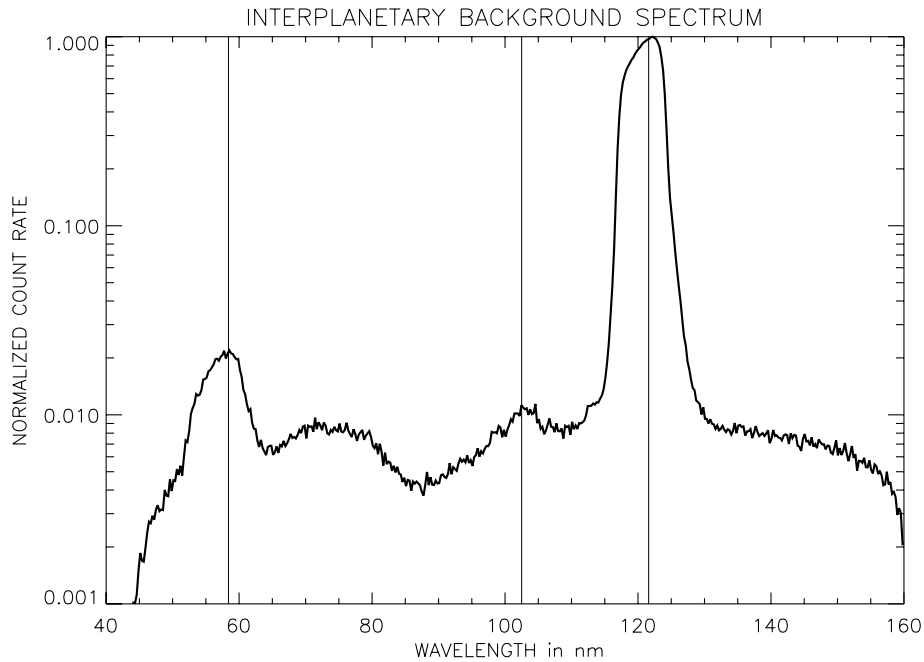

Figure 2. Normalized count rate obtained when observing the interplanetary background with the EUV channel of PHEBUS. The channel covers the spectral range from 55 to 155 nm. The H Lyman α (121.6 nm), H Lyman β (102.5 nm) and He 58.4 nm lines are indicated by vertical lines. The observations were done with the large aperture (slit removed) which degrades the resolution by a factor of 14 but increases the count rate by a factor 20. The helium line at 58.4 nm is clearly visible. The bump from 65 to 85 nm (not observed in ground measurements) is caused by reflections inside the instrument which occur when the slit is removed.

helium line (58.4 nm) counts, hydrogen (121.6 nm) counts respectively. Each individual measurement corresponds to a cumulation time of 21 s. The calibration factor at 58.4 nm provided in the headers of the files is equal to 0.36 counts per second.

For each Roll Calibration Maneuver, called RCM 1 to 4 below, we have estimated the helium line excitation rate at 1 AU based on the values obtained in the previous paragraph. Then for each measurement, we have used the Lallement et al. (2004) model to estimate the interplanetary helium background intensity. The ratio between the measured count rates and the model values gives an estimate of the calibration factor of the helium channel independently from the published UVS calibration.

The parameters for each RCM are given in Table 1. A comparison between the UVS data and our model in the case of RCM 4 are shown in Figure 3. For the first 3 maneuvers, we derive a calibration factor equal to 0.41 ± 0.08 counts per Rayleigh for the helium channels. The uncertainty corresponds to 1-σ. The 4th RCM gives a slightly higher ratio of 0.45 but still compatible within uncertainties.

As shown in Figure 3, the model represents well the general variation of the data between low and high values which validates our approach. RCM 4, shown in Figure 3, has the largest variations of the 4 maneuvers. By averaging the calibration factors derived for the 4 RCM, we find a value of 0.42 ± 0.04 which is close to the calibration factor of 0.36 counts per second per Rayleigh given by the UVS/Mariner 10 team.

In conclusion, the comparison between our model of interplanetary glow (Lallement et al., 2004) and the UVS data obtained during 4 maneuvers performed before the Mercury flybys of Mariner 10 has allowed us to derive the calibration factor of the helium channel of the UVS. This value is slightly different from the published calibration factor. The ratio is equal to 1.16. We conclude that our approach is valid and can be applied to the calibration of the PHEBUS instrument.

3.2. Calibration of PHEBUS at 58.4 nm

The PHEBUS instrument is dedicated to the study of the exosphere of Mercury. It is a double channel UV spectrograph covering a spectral range from 50 to 320 nm. Due to various constraints before the launch, the

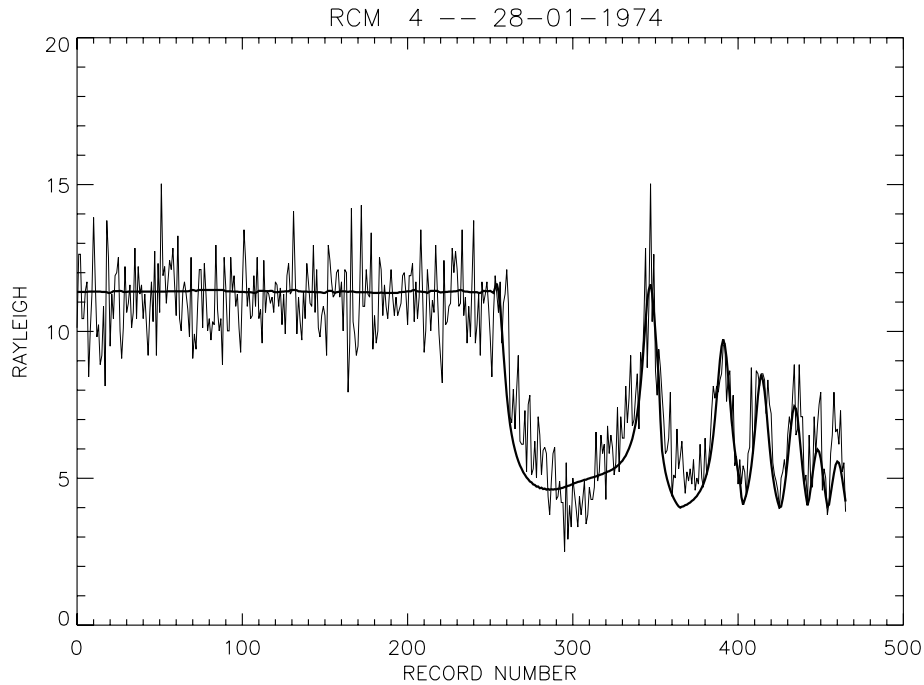

Figure 3. Comparison between UVS/Mariner 10 data and our model computations for RCM 4. The horizontal axis is the record number, the vertical axis is in Rayleigh. This maneuver has the largest variation between high and low values of the 4 maneuvers discussed here. These variations are caused by the change in look direction of the instrument during the spacecraft roll. The calibration factor is obtained by a linear regression between data and model. In this particular case, we find a calibration factor equal to 0.45 ± 0.08 counts per second per Rayleigh.

short wavelength channel (50–155 nm) was not fully calibrated on the ground although a radiometric model was derived from ground measurements of the reflectivity of the optical parts. Here, we will use the method validated with the UVS/Mariner 10 data to calibrate the short wavelength channel of PHEBUS at 58.4 nm.

In 2021, during the cruise of Bepi-Colombo to Mercury, it has been possible to perform 13 observations of the interplanetary ultraviolet glow at 58.4 nm. Table 2 gives the parameters of these observations, date, position of the spacecraft, PHEBUS boresight, observed count rate, statistical uncertainty and the result of the IP He model.

Table 2
Parameters of the PHEBUS Interplanetary Observations

Date	MPO R(AU)	MPO lon (°)	MPO lat (°)	LOS lon (°)	LOS lat (°)	Count rate (s^{-1})	Model (R)
2021-02-14	0.595	273.3	−1.0	333.7	−71.9	1.97 ± 0.14	3.5
2021-02-14	0.595	273.4	−1.0	197.3	−45.5	1.60 ± 0.14	3.5
2021-02-17	0.580	280.1	−1.4	0.7	−3.0	3.17 ± 0.08	3.6
2021-03-30	0.546	33.3	−2.4	104.6	48.0	5.85 ± 0.12	5.1
2021-03-30	0.547	33.3	−2.4	112.6	−5.2	12.47 ± 0.15	11.3
2021-03-30	0.547	33.4	−2.4	110.8	−44.3	7.28 ± 0.14	6.0
2021-06-26	0.840	170.4	3.4	251.0	7.1	1.89 ± 0.18	3.0
2021-10-09	0.325	18.6	−4.1	304.6	−2.2	6.59 ± 0.14	6.1
2021-10-09	0.325	18.7	−4.1	304.7	−2.3	6.52 ± 0.14	6.1
2021-10-09	0.325	18.8	−4.1	304.8	−2.3	6.34 ± 0.14	6.1
2021-10-09	0.322	24.2	−3.5	305.7	−2.2	6.20 ± 0.13	6.1
2021-10-09	0.322	24.3	−3.5	305.7	−2.7	6.16 ± 0.13	6.1
2021-10-10	0.322	24.4	−3.5	305.8	−2.6	6.12 ± 0.13	6.1

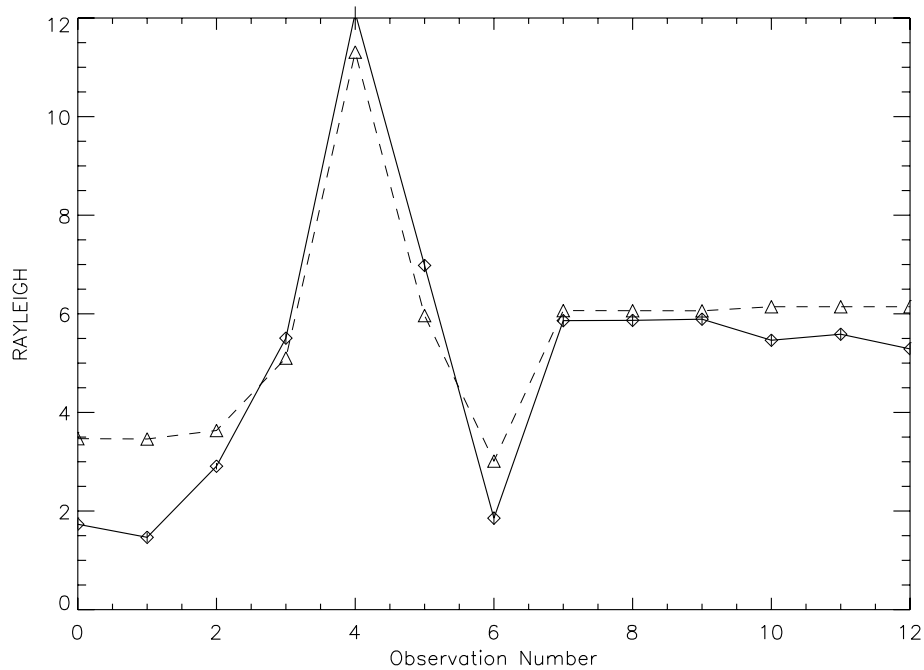

Figure 4. Comparison between PHEBUS observations of the interplanetary background at 58.4 nm and model computations. The data are shown by the diamonds and the solid line. The model values are shown by the triangle and the dashed line. The numerical values are given in Table 2. The highest value correspond to a line of sight crossing the helium focusing cone in the downwind region. The first two observations are significantly lower than the model prediction, suggesting that the ionization rate in this analysis should be revised. However, it does not affect the derivation of the calibration factor at 58.4 nm of PHEBUS significantly.

The excitation rate at 1 AU for each observation has been computed using the MgII proxy correlated to the CDS/SOHO data (McMullin et al., 2004), as shown in Figure 1.

From the linear regression performed on the data and model, as shown in Figure 4, we find that the PHEBUS calibration factor at 58.4 nm is equal to 1.06 count s^{-1} per Rayleigh.

By only taking into account the measurement uncertainties given in Table 2, we obtain a 1-σ uncertainty equal to 0.02 count s^{-1} per Rayleigh. However, the total uncertainty must include the systematic uncertainty due to the model. Its main source of uncertainty is due to the uncertainty of the neutral helium density in the interstellar medium. Möbius et al. (2004) give a relative uncertainty equal to 0.13 for this value. Since the interplanetary background model at 58.4 nm is optically thin, this can be propagated to the calibration factor. In the end, we estimate that the uncertainty is equal 0.14 count s^{-1} per Rayleigh.

It should be noted that the radiometric model of PHEBUS, based on ground measurements of the optical elements is in agreement with this value. We conclude that no significant degradation has been observed since launch.

4. Flyby Description and Results

The first flyby of Mercury by the Bepi-Colombo mission occurred on 1 October 2021. During the whole sequence, the spacecraft was kept in inertial attitude with the radiator side pointing away from the Sun. The spacecraft approached from the nightside of Mercury, crossed the shadow of the planet, then moved to the dayside. The closest approach to the surface, just below 200 km, happened a few minutes before the spacecraft crossed the terminator. The closest point of the planet was in the southern hemisphere roughly at mid-latitude.

The PHEBUS instrument was switched on 30 min before closest approach. The observation sequence lasted for 1 hour. Three channels operated throughout the observation, the two visible channels at 404 and 422 nm and the short wavelength UV channel (50–155 nm). Here, we present the HeI 58.4 nm data.

The geometry is described in Figure 5. The left panel shows the view as seen from the Sun. The red curve is the trajectory of the spacecraft. The gray arrows show the PHEBUS boresight. The closest approach, shown by the

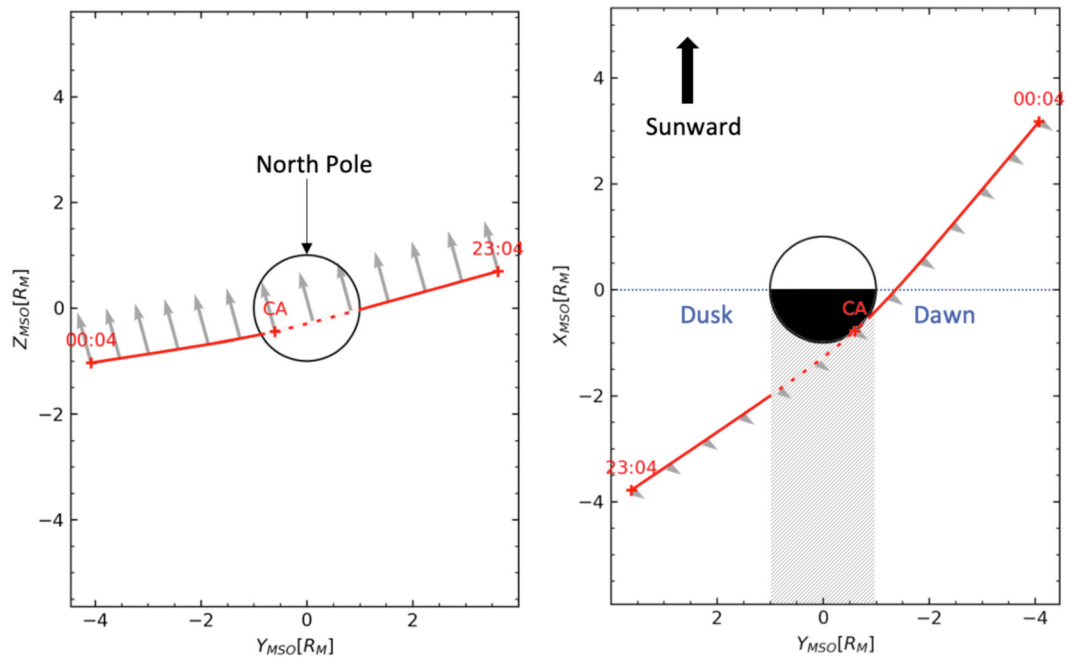

Figure 5. Plots of the geometry of the first flyby of Mercury by Bepi-Colombo. The red line shows the trajectory of BC while the gray arrow corresponds to the boresight of PHEBUS. The left panel shows the view from the Sun. The right panel shows the view looking down on Mercury's orbit plane. Mercury Solar Orbital (MSO) coordinates are defined as, XMSO is positive sunward, ZMSO is positive northward, aligned with Mercury's spin axis, and YMSO is positive duskward.

letters CA and the red cross, is on the nightside of Mercury. We see that the spacecraft passes at mid-latitude and that the look direction is fixed during the whole sequence, roughly pointing to the north ecliptic pole. The right panel shows the view looking down on Mercury's orbit plane. The nightside of Mercury is shown by the black half-disk and the shadow of Mercury is shown by the shaded area on the side opposite from the Sun. Dusk and Dawn regions are also indicated. The path of the spacecraft goes through the shadow into the dawn region.

The position of the scanner was chosen to optimize the count rate while avoiding the illumination of the PHEBUS field of view by the dayside surface. Note also, that PHEBUS which is mounted on the radiator side is always on the opposite side from the Sun. The angle between the Mercury to Bepi-Colombo vector and the boresight is slightly larger than 90°. After crossing the terminator, Bepi-Colombo flew through the dawn region.

The count rate measured by the short wavelength channel of PHEBUS is shown in Figure 6. The plot covers the whole observation sequence. The shaded area (dotted line) corresponds to the times when Bepi-Colombo is in the shadow of Mercury. The time origin (zero value) corresponds to the time when the spacecraft is at closest approach. The solid line shows the count rate as a function of time. Count rates vary between 6 and 14 counts per second. The sampling interval is 10 s. The integration time for each individual measurement is equal to 8 s as the two remaining seconds are used by the instrument to process the detector images and transfer them to the spacecraft. The thicker solid line shows a 5-sample running average. The two lighter solid lines show the 1-σ uncertainty for the average obtained by error propagation of the individual measurements.

The emissions measured during the flyby correspond to two sources. Away from the planet, the count rates are caused by the backscattering of solar photons by interplanetary helium atoms. We see that the emission at 58.4 nm is roughly constant for the first 30 min of the observation at about 9 counts per second. At the shadow entry, we see a small deep which could be linked to the helium exosphere in the tail region of Mercury. Unfortunately, the signal to noise ratio is quite low and we will wait for the orbital phase of the mission to study this in more detail. Once the spacecraft comes out of the shadow, we see a sharp increase of about 5 counts per second and then a decrease as the distance between the spacecraft and the planet increases. Ten minutes after Closest Approach, the count rate is back to 9 counts per second in average. The average count rate due the interplanetary emission at 58.4 nm is almost twice as large as the peak of exospheric emission which suggests that the exospheric signal is lower by almost half than the interplanetary emission.

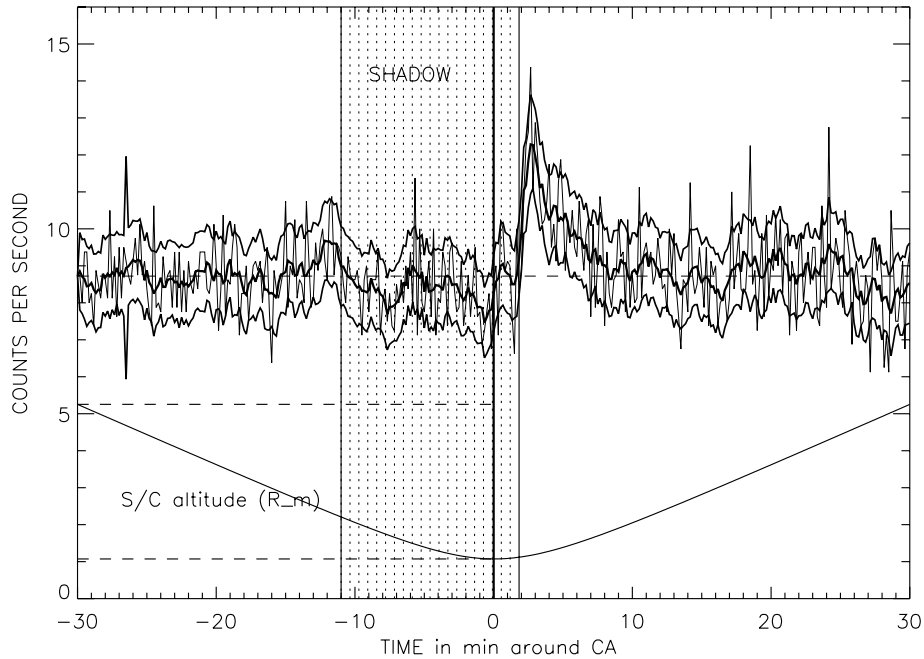

Figure 6. Plot of the count rate at 58.4 nm recorded by PHEBUS during the flyby of Mercury. The shaded area labeled "SHADOW" shows the time when Bepi-Colombo is in the shadow of the planet. The solid line at the bottom gives the distance to the planet center in units of radius of Mercury (values between 1 and 5). The thickest line corresponds to a running average over 5 samples. The thin lines show the 1-sigma uncertainty curves for the running average. The mean value for the interplanetary background is shown by the horizontal dashed line.

From the reconstruction of the geometry and after applying the calibration factor derived in the previous section, we can plot the 58.4 nm exospheric signal as a function of altitude of the spacecraft. Note that because of the chosen scanner position, the lowest altitude on the line of sight is at the spacecraft. Therefore, we do not use the impact parameter of the line of sight but the spacecraft altitude in the plot. We find that below 450 km of altitude the line of sight is not completely out of the shadow. Above 450 km, the count rate starts to decrease. From Figure 7, we see that the exospheric brightness reaches 4 R at 470 km. For a similar altitude, (Broadfoot et al., 1976) reported a value of 30 R observed by UVS on Mariner 10. Their measurements were obtained for a subsolar point. The PHEBUS observation were made with a solar zenith angle decreasing between 85° and 75°. The ratio between the Mariner 10 estimate and our observation is approximately equal to 6. However, this value should be taken with precaution. The PHEBUS measurements were made close to the tangent point of the line of sight while the UVS ones were made farther away from the tangent point. We have estimated that the PHEBUS brightness values should be multiplied by a factor of 1.7 to correct for this. We will come back to this difference below.

We have tried to fit the profile shown in Figure 7 with a Chamberlain model (Brandt & Chamberlain, 1959) to check whether we can derive the number density and temperature at the exobase of Mercury. To do this, we have computed a series of Chamberlain profiles with temperatures, noted T_{ex}, ranging from 300 to 800 K, assuming that the exobase is at the surface of Mercury. To compute the brightness, we have assumed that the exosphere is optically thin at 58.4 nm. This can be verified by computing the typical brightness for an optical thickness at line center of 0.1 which can be considered as the limit for this assumption. For an helium exosphere at 575 K, the line center cross section is equal to 1.57×10^{-13} cm^2. Assuming that the excitation rate at 1 AU is equal to 10^{-5} s^{-1} and that the distance of Mercury to the Sun is 0.38 AU, we find that an optical thickness of 0.1 corresponds to a brightness of 44 R which is higher than the values we consider here. For each individual measurement, we have computed the intensity along the line of sight using the exact geometry. For each set of intensity model, we have derived the exobase density, noted N_{ex}, by linear regression between calibrated data and model. Finally we have estimated the quality of the fit by estimating the quantity χ^2,

$$\chi^2 = \left(\frac{1}{N-1}\right)\Sigma_i \frac{(D_i - M_i)^2}{(\sigma_i)^2}$$

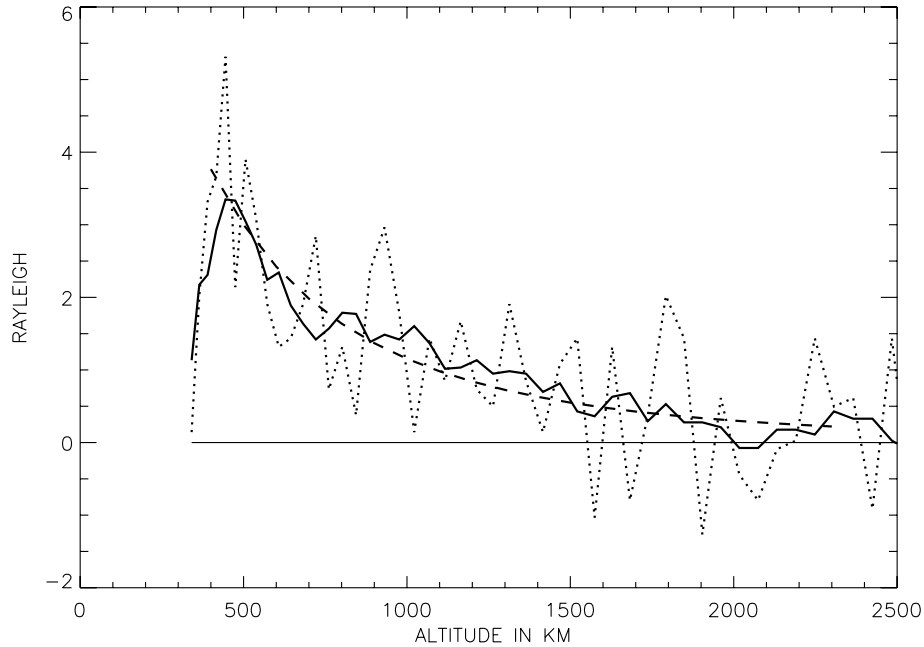

Figure 7. Altitude profile of the intensity recorded in the dawn region after the crossing of the shadow of the planet. Only lines of sight that are completely outside of the shadow are shown. The data are shown by the dotted line, the solid line is a running average on 5 samples. The dashed line is a fit of the intensity profile based on a Chamberlain density profile with $T = 575$ K at the ground. See text for details of computation.

Where, (D_i) represents the calibrated measurements, (σ_i) the uncertainty of each measurement and (M_i) is the modeled intensity for each measurement. N is the number of independent measurements, about 40. Note that the model has two parameters, the temperature and density at the exobase. However, since the model is optically thin, the exobase density is defined by the exobase temperature. As a result, there is only one free parameter. Note that we have used an excitation rate at 1 AU equal to 0.8×10^{-6} s^{-1}. For the exospheric emission, the excitation rate was scaled to the distance of Mercury to the Sun, that is, 0.371 AU, which gives a value of 5.8×10^{-6} s^{-1}.

The results of our computations are given is Table 3. The minimum value of χ^2 is 1.33 and corresponds to an exobase temperature of 500 K. From the values in the table, we can estimate that the best fit is obtained in the temperature range of 450–550 K. We also see from the lowest value of χ^2 that there is room for improvement of the fit. The corresponding density at the exobase is between 625 cm^{-3} and 1,000 cm^{-3}.

Table 3
Estimate of the Helium Temperature and Density at the Exobase

T_{ex} (K)	N_{ex} (cm^{-3})	χ^2
200	13,362	2.87
250	5,714	2.42
300	3,121	2.02
350	1967	1.71
400	1359	1.49
450	1002	1.37
500	777	1.33
550	625	1.36
600	519	1.42
650	442	1.50
700	385	1.58

Following the Mercury flybys of Mariner 10, Broadfoot et al. (1976) found an exobase temperature of 575 K with an exobase density of 4,500 cm^{-3}. In Figure 7, we have added a model of the intensity computed in the case of an exobase temperature of 575 K. We see that the fit is acceptable given the large uncertainties of our measurements. However, as stated above, the intensities recorded by PHEBUS are significantly lower than the UVS measurements. Assuming a temperature of 575 K, we find a ground density close to 600 cm^{-3}, which is a factor of 7 lower than the estimate from Broadfoot et al. (1976). If we consider our best fit value of 777 cm^{-3} and 500 K, the ratio is close to 6.

In conclusion, we have been able to reconstruct the altitude profile of helium density in the exosphere of Mercury from the data recorded by PHEBUS during the first flyby of Bepi-Colombo. We have used the formalism developed by Brandt and Chamberlain (1959) to estimate the temperature and the density of helium at the exobase (i.e., the ground in this case). The best fit was obtained for a temperature in the range of 450–550 K and a density in the range of 600 cm^{-3} to 1,000 cm^{-3}.

The temperature we find is close to the value found by the UVS team on Mariner 10. On the other hand, our density estimate is 4.5–7.5 times lower than the one based on the Mariner 10 data. The PHEBUS observation during this flyby was restricted to the dawn region of the exosphere with a solar zenith angle between 75° and 85° while the UVS data correspond to the sub-solar region. This will be discussed in the next section.

5. Discussion

The data of the PHEBUS channel at 58.4 nm (helium resonance line) obtained during the first flyby of Mercury by Bepi-Colombo have been analyzed. Following Chamberlain's approach, we have been able to derive the exobase density and temperature that fit the PHEBUS data. We find values between 450 and 550 K for the temperature and between 600 cm^{-3} and 1,000 cm^{-3} for the density.

Broadfoot et al. (1976) found an exobase temperature of 575 K with an exobase density of 4,500 cm^{-3} by analyzing the UVS Mariner 10 data. The Mariner 10 value is 4.5–7.5 times larger than our result. On the other hand, the PHEBUS altitude profile is consistent with an exobase temperature which is close to the value deduced by Mariner 10.

By carefully comparing the response of both instruments to the interplanetary background emissions at 58.4 nm, we have shown that their respective calibrations are not the source of this discrepancy.

Mariner 10 flybys and the first Bepi-Colombo flyby were performed at times close to a minimum of solar activity, which means that both photo-ionization rates and excitation rates of the helium 58.4 nm line were close to minimum values and cannot explain such a large difference.

Below, we consider some possible explanations for the variation of helium content in the exosphere of Mercury.

5.1. Geometry of Observation

First, we should consider the possibility that the difference between UVS and PHEBUS measurements is simply caused by a possible variation in helium distribution with local time. The Mariner 10 measurements correspond to sub-solar altitude profiles (noon local time) whereas the PHEBUS helium observations were performed for a local time close to 07:00, that is, just after the terminator. However, Leblanc and Chaufray (2011) modeled helium altitude profiles for different local hours assuming exobase densities and temperatures varying as a function of the local time. Their conclusion was that there is little variation in density profiles on the dayside as temperature effects tend to smooth out variations from the source terms. On the night side, the model showed an accumulation of helium close to the surface leading to larger densities at dawn and dusk which is the opposite of what we are observing here. Fortunately, future PHEBUS observations will allow us to verify this point as the spacecraft trajectory will cover all local times during the nominal mission.

Chamberlain (1990) estimated that the anisotropy of the resonance scattering for the He 58.4 nm line could be as high as a factor of 2 between colinear and perpendicular scattering. For the Bepi-Colombo data, the PHEBUS observing geometry indeed corresponds to a perpendicular scattering but as shown in Figure 2 of Broadfoot et al. (1976), this is also the case for the Mariner 10 flybys so both data sets would be affected in the same way. The discrepancy cannot be explained that way.

5.2. Width of the Solar Line

Yoneda et al. (2021) suggested that the solar line width at 58.4 nm could be smaller than previously assumed. They quoted a possible width of 0.0016 nm instead of the value of 0.015 nm generally used. Here for instance, we have used the value of 0.0135 nm derived from the SUMER/SOHO measurements (Wilhelm et al., 1997). The smaller value corresponds to a Doppler shift of 4.1 km/s while the standard value is almost 10 times larger. In the case of the first flyby of Mercury by Bepi-Colombo, the radial velocity of the planet was close to 10 km/s while the radial velocity of Mercury was close to zero during the Mariner 10 flybys. Let us assume that the apparent decrease is simply due the change of solar illumination because of a narrow solar line. In that case, the reduction of intensity by a factor of 6 corresponds to the factor $R = e^{-\left(v_r/\Delta v_d\right)^2}$ where v_r is the radial velocity of the exosphere and Δv_d is the equivalent Doppler width of the solar line (see Appendix A). We can show that $\Delta v_d = v_r/(-\ln(R))^{1/2}$ with R equal to 1/6. This yields a value of Δv_d equal to 7.5 km/s.

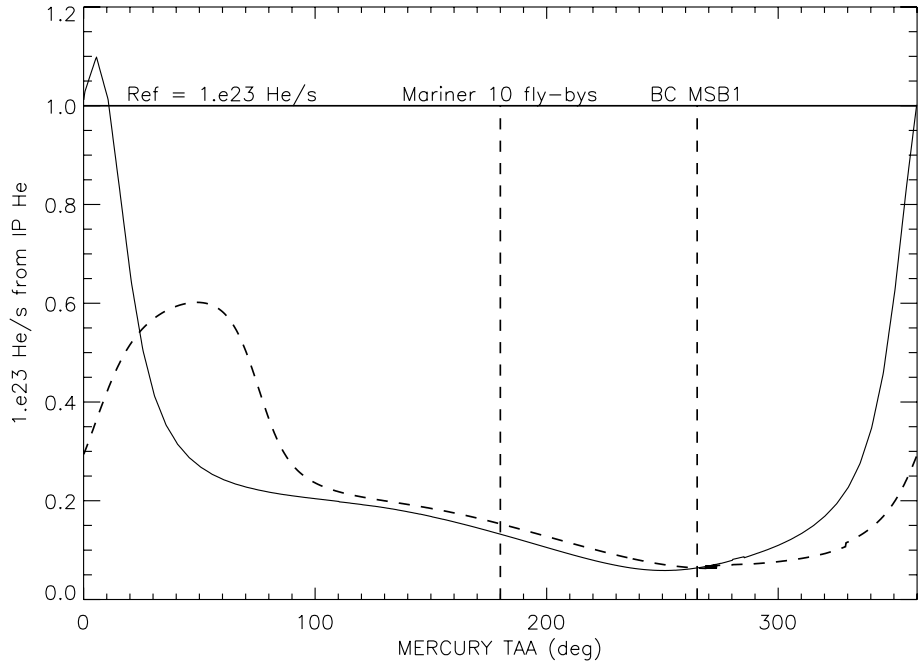

Figure 8. Flux of interplanetary helium atoms impacting the surface of Mercury as a function of the True Anomaly Angle of Mercury (solid line). The dotted line at the top marks the reference flux of 10^{23} He/s estimated from the Mariner 10 profile. The computed IP He flux reaches this value when Mercury crosses the helium cone (TAA = 7 deg). The TAA of Mercury for the Mariner 10 and Bepi-Colombo flybys are indicated. The dashed line is an average of the IP He flux for the 10 days preceding the date. In that case, the peak flux is shifted by 40°.

However, such a narrow width for the illuminating solar line at 58.4 nm is inconsistent with observations of the interplanetary glow at 58.4 nm. Interstellar helium atoms have a bulk velocity of 25 km/s (Möbius et al., 2004) in the solar rest frame. When approaching the inner heliosphere, their velocity is not significantly modified. This means that helium atoms in the upwind region have a Doppler shift in the solar rest frame of the order of 25 km/s, significantly larger than the value of 7.5 km/s found above. In the case of a narrow solar line, these atoms should not backscatter solar photons. Yet, as shown in Table 2, PHEBUS has observed the interplanetary glow at 58.4 nm in the upwind direction three times in February 2021. From this, we can conclude that the width of the solar line at 58.4 nm is equivalent to a Doppler shift larger than 25 km/s and that the change in exospheric HeI intensity between the Mariner 10 and Bepi-Colombo flybys is not due to a narrow solar line at 58.4 nm.

5.3. Contribution of Interplanetary Helium

Finally, we should consider the possibility that a fraction of helium atoms in the exosphere of Mercury originate from the interstellar medium. It is usually assumed that helium atoms originate from the solar wind. As stated in Leblanc and Chaufray (2011), the flux of helium in the solar wind at Mercury corresponds to 10^{25} He/s. However, these particles are ionized and therefore are filtered by the magnetosphere of Mercury. They mainly impact the surface of Mercury at the magnetospheric cusps. Leblanc and Chaufray (2011) also showed by modeling that a flux of 10^{23} He/s is enough to explain the helium content in the exosphere as measured by Mariner 10. Therefore, by analogy with the Moon, they concluded that the solar wind is the most likely source for helium. This means that roughly 1% of the α particles (He^{2+}) in the solar wind reach the surface of Mercury and are released in the exosphere after impact.

We have computed the flux of neutral helium atoms that reach the surface of Mercury due to the relative motion between the planet and the interstellar helium flow (Figure 8). These particles are neutral and are not filtered by the magnetosphere, therefore their distribution on the surface should be much more uniform than in the case of α particles. The bulk flow of interstellar helium in the solar rest frame is aligned with the direction defined in ecliptic coordinates by $\lambda, \beta = 254, +6$ deg (Möbius et al., 2004). The bulk velocity is constant and close to 26 km/s. As Mercury rotates around the Sun, the relative velocity changes from roughly 20 km/s to 80 km/s. This means that the flux of interstellar helium impacting the surface of Mercury varies with the position of Mercury with

respect to the direction of the flow of the interstellar gas. This flux never goes to zero as the velocity of Mercury is significantly larger than the velocity of the interplanetary gas. As shown in Figure 10 of Quémerais et al. (2020), the interplanetary helium density is not constant along the orbit of Mercury either but peaks strongly at the helium focusing cone downwind behind the Sun, where helium atoms are gravitationally focused. The number of helium atoms impacting the surface is obtained by multiplying the flux of IP He by the cross-section of Mercury. We see that the flux reaches the value of 10^{23} He/s when the planet crosses the helium focusing cone. At its peak, the flux of interplanetary helium has a contribution equivalent to the estimate of the solar wind contribution, which means that both contributions must be taken into account. At the position of the BC flyby (265°), the IP He flux is 10 times lower than the peak value and is significantly lower than the estimated contribution of the solar wind α particles. The result of this computation cannot explain the difference by a factor of 6 between Mariner 10 and Bepi-Colombo measurements, as the ratio of IP He flux values is close to 2. It shows however that helium atoms from the interstellar medium are a potential source for helium in the exosphere and may explain a part of the variability of the helium content in the exosphere of Mercury.

5.4. Conclusion

By mapping the exospheric helium content as a function of the TAA of Mercury on its orbit and of the local time for similar TAA values, we will be able to differentiate between the source terms. It should be noted also that the helium atoms have a lifetime against photo-ionization at Mercury which is close to 10^6 s, that is, close to 10 days. In that case the peak for the IP He flux will be shifted by 40° as shown by the dashed line in Figure 8.

The values discussed here are preliminary estimates and more detailed modeling is required to understand the various contributions to the exosphere. These open questions show the importance of future observations of helium atoms in the exosphere of Mercury. During the orbital phase of the Bepi-Colombo mission, it will be possible to cover all TAA and local time values.

Appendix A: Computation of the Solar Excitation Rate

The excitation rate of a resonance line is given by the product of the solar flux at line center by the total scattering cross section.

From Mitchell et al. (1934), and adapting the units to the international system, we can write

$$\sigma_{tot} = \int_{-\infty}^{+\infty} \sigma(\nu)\ d\nu = \frac{1}{4\pi\ \epsilon_o}\ \frac{\pi\ q^2}{m_e\ c}\ f \tag{A1}$$

Where ν is the frequency, $\sigma(\nu)$ the scattering cross section as a function of frequency, q the charge of an electron, m_e mass of an electron, c the speed of light and f the oscillator strength of the resonance line.

ϵ_o is defined by

$$\epsilon_o = \frac{1}{\mu_o\ c^2} = \frac{10^7}{4\pi\ c^2} \tag{A2}$$

If we express the line center flux in units of wavelength, the total scattering cross section is scaled by $\frac{\lambda^2}{c}$ where λ is the wavelength of the considered line.

In the case of the He line at 58.4 nm, the oscillator strength is given as $f = 0.27$ (Wiese & Fuhr, 2009) which gives,

$$\sigma_{tot} = 8.34 \cdot 10^{-16} \mathrm{cm}^2\ \text{Å}$$

The excitation rate g is given as,

$$g = F_o \cdot \sigma_{tot}$$

Where F_o is the line center flux expressed in units of $\mathrm{cm}^{-2}\ \mathrm{s}^{-1}\ \text{Å}^{-1}$.

Measuring the line center flux requires a very high spectral resolution, at least 10^5, which is extremely demanding in the ultraviolet. However, if the line shape is known or assumed, it is then possible to express the line center flux

as a function of the integrated flux. If we assume that the shape of the 58.4 nm line is a Gaussian with a known Full Width at Half Maximum, we can write

$$F(\lambda) = F_o \cdot e^{-\left(\frac{\lambda}{\Delta\lambda}\right)^2}$$

The Full Width at Half Maximum, *FWHM*, is equal to

$$FWHM = 2 \cdot \sqrt{\ln 2} \cdot \Delta\lambda$$

The relation between the line center flux F_o and the integrated flux F_{tot} is given by

$$F_o = \frac{F_{tot}}{\Delta\lambda \cdot \sqrt{\pi}} = F_{tot} \cdot \frac{2 \cdot \sqrt{\ln 2}}{FWHM \cdot \sqrt{\pi}} \quad \text{(A3)}$$

Data Availability Statement

The Mercury Swing-By 1 data for the HE 58.4 nm line and the geometry information are available at (Quémerais, 2023). The UVS/Mariner 10 data were provided by NSSDCA (NASA Space Science Data Coordinated Archive). The data can be obtained by contacting the curator of the archive, see the following page for details on these data: https://nssdc.gsfc.nasa.gov/nmc/dataset/display.action?id=PSPA-00315.

Acknowledgments
The BepiColombo mission to explore Mercury is an international cooperation between the European Space Agency, ESA, and the Japan Aerospace Exploration Agency, JAXA. The PHEBUS project is funded by National Space Agencies of France, Japan, and Russia. We thank Terry Forrester at the Lunar and Planetary Laboratory in Tucson for his help in understanding the Mariner 10 data.

References

Brandt, J. C., & Chamberlain, J. W. (1959). Interplanetary gas. I. Hydrogen radiation in the night sky. *The Astrophysical Journal*, *130*, 670. https://doi.org/10.1086/146756

Broadfoot, A. L., Shemansky, D. E., & Kumar, S. (1976). Mariner 10: Mercury atmosphere. *Geophysical Research Letters*, *3*(10), 577–580. https://doi.org/10.1029/GL003i010p00577

Chamberlain, J. W. (1990). Calculation of polarization and anisotropy of resonant and fluorescent scattering. *Icarus*, *84*(1), 106–117. https://doi.org/10.1016/0019-1035(90)90161-2

Chassefière, E., Maria, J. L., Goutail, J. P., Quémerais, E., Leblanc, F., Okano, S., et al. (2010). PHEBUS: A double ultraviolet spectrometer to observe Mercury's exosphere. *Planetary and Space Science*, *58*(1–2), 201–223. https://doi.org/10.1016/j.pss.2008.05.018

Dalaudier, F., Bertaux, J. L., Kurt, V. G., & Mironova, E. N. (1984). Characteristics of interstellar helium observed with Prognoz 6 58.4-nm photometers. *Astronomy and Astrophysics*, *134*(1), 171–184.

Killen, R., Shemansky, D., & Mouawad, N. (2009). Expected emission from Mercury's exospheric species, and their ultraviolet-visible signatures. *The Astrophysical Journal Supplement*, *181*(2), 351–359. https://doi.org/10.1088/0067-0049/181/2/351

Kumar, S., & Broadfoot, A. L. (1979). Signatures of solar wind latitude structure in interplanetary Lyman-alpha emissions: Mariner 10 observations. *The Astrophysical Journal*, *228*, 302–311. https://doi.org/10.1086/156847

Lallement, R., Raymond, J. C., Vallerga, J., Lemoine, M., Dalaudier, F., & Bertaux, J. L. (2004). Modeling the interstellar-interplanetary helium 58.4 nm resonance glow: Towards a reconciliation with particle measurements. *Astronomy and Astrophysics*, *426*(3), 875–884. https://doi.org/10.1051/0004-6361:20035929

Leblanc, F., & Chaufray, J. Y. (2011). Mercury and Moon He exospheres: Analysis and modeling. *Icarus*, *216*(2), 551–559. https://doi.org/10.1016/j.icarus.2011.09.028

McMullin, D. R., Bzowski, M., Möbius, E., Pauluhn, A., Skoug, R., Thompson, W. T., et al. (2004). Heliospheric conditions that affect the interstellar gas inside the heliosphere. *Astronomy and Astrophysics*, *426*(3), 885–895. https://doi.org/10.1051/0004-6361:20047147

Mitchell, A. C. G., Zemansky, M. W., & Keenan, P. C. (1934). REVIEW: Resonance radiation and excited atoms. *The Astrophysical Journal*, *80*, 77. https://doi.org/10.1086/143583

Möbius, E., Bzowski, M., Chalov, S., Fahr, H. J., Gloeckler, G., Izmodenov, V., et al. (2004). Synopsis of the interstellar He parameters from combined neutral gas, pickup ion and UV scattering observations and related consequences. *Astronomy and Astrophysics*, *426*(3), 897–907. https://doi.org/10.1051/0004-6361:20035834

Quémerais, E. (2023). Phebus observation of helium during the first fly-by of mercury [Dataset]. LATMOS. Retrieved from http://doi.latmos.ipsl.fr/phebus-euv-mercury-swingby1-heline-latmos.html

Quémerais, E., Chaufray, J.-Y., Koutroumpa, D., Leblanc, F., Reberac, A., Lustrement, B., et al. (2020). PHEBUS on Bepi-Colombo: Post-launch update and instrument performance. *Space Science Reviews*, *216*(4), 67. https://doi.org/10.1007/s11214-020-00695-6

Vallerga, J., Lallement, R., Lemoine, M., Dalaudier, F., & McMullin, D. (2004). EUVE observations of the helium glow: Interstellar and solar parameters. *Astronomy and Astrophysics*, *426*(3), 855–865. https://doi.org/10.1051/0004-6361:20035887

Weller, C. S., & Meier, R. R. (1974). Observations of helium in the interplanetary/interstellar wind: The solar-wake effect. *The Astrophysical Journal*, *193*, 471–476. https://doi.org/10.1086/153182

Wiese, W. L., & Fuhr, J. R. (2009). Accurate atomic transition probabilities for hydrogen, helium, and lithium. *Journal of Physical and Chemical Reference Data*, *38*(3), 565–720. https://doi.org/10.1063/1.3077727

Wilhelm, K., Lemaire, P., Curdt, W., Schühle, U., Marsch, E., Poland, A. I., et al. (1997). First results of the SUMER telescope and spectrometer on SOHO—I. Spectra and spectroradiometry. *Solar Physics*, *170*(1), 75–104. https://doi.org/10.1023/A:1004923511980

Woods, T. N., Eparvier, F. G., Hock, R., Jones, A. R., Woodraska, D., Judge, D., et al. (2012). Extreme ultraviolet variability experiment (EVE) on the solar dynamics observatory (SDO): Overview of science objectives, instrument design, data products, and model developments. *Solar Physics*, *275*(1–2), 115–143. https://doi.org/10.1007/s11207-009-9487-6

Yoneda, M., Dima, G., & Berdyugina, S. V. (2021). Mercury's exospheric He I 58.4 nm emission: Dependence on the orbital phase. *Astronomy and Astrophysics*, *654*, L7. https://doi.org/10.1051/0004-6361/202142155